Structure and Dynamics of Dilute Polymer Solutions under Shear Flow via Nonequilibrium Molecular Dynamics

C. Aust,*,† M. Kröger,†,‡,§ and S. Hess†

Institut für Theoretische Physik, Technische Universität Berlin, PN 7-1, Hardenbergstr. 36, D-10623 Berlin, Germany; Fritz Haber Research Center and Department of Physical Chemistry, The Hebrew University, IL-91904 Jerusalem, Israel; and Institute of Polymers, Polymer Physics, ML H 18, Sonneggstr. 3, ETH Zentrum, CH-8092 Zürich, Switzerland

Received October 27, 1998; Revised Manuscript Received April 13, 1999

ABSTRACT: We present and discuss results obtained by an extensive nonequilibrium molecular dynamics computer simulation study of polymer solutions under shear, where the chain consists of N beads connected by a finitely extendable nonlinear elastic (FENE) spring force and the solvent is explicitly taken into account. Various scaling laws are extracted from the data which allow one to predict the qualitative− and to certain extent also quantitative−structural and rheological behavior of polymer solutions under good solvent conditions. For most quantities, the results drawn from simulation are compared with experimental data and theoretical predictions which are based on similar models (e.g., harmonic bond potentials or Brownian dynamics methods). Specifically, and in contrast to common theoretical approaches, the simulation yield information about a set of different but characteristic relaxation times, which determine the rheological and structural behavior (for example, flow birefringence, structure factor, rotational dynamics) separately, the difference either resulting from the underlying static or dynamic nature or from relaxation processes which act on different length scales.

1. Introduction

The flow behavior of viscoelastic fluids, in particular of polymer solutions, is more complex than that of the familiar Newtonian fluids. To be more specific, shear thinning and the Weissenberg effect[1] are typical phenomena which are of great technological importance. These effects are found to be strongly correlated with flow-induced conformational changes of the dissolved polymer chains and they can be dramatic in dilute solutions. The orientation and deformation of chain molecules can and have been measured in flow birefringence,[2,3] light scattering,[4,5] and neutron scattering[6] experiments and can also be studied by computer simulation methods of the kind to be used here.

The aim of the theory is to predict the flow behavior and structural changes for given microscopic models. Analytical kinetic theories for the dynamics of polymers are restricted to rather simple models, and approximations have to be made, such as single-chain or mean-field approaches. One major aim of the theory is also to relate the structural properties with the rheological information. This causes some difficulties for simple theories, but nevertheless, many analytic expressions exist which predict the rheological behavior of polymer chains in solution and their structural properties.[1,7] Within a limited range of applicability, these theories are quite useful. In the case of steady shear flow, they yield the dependence of many measurable quantities on the chain length, N (or molecular weight M), and on the shear rate, γ, which often can be expressed in terms of power laws. Such power-law behavior is well-known from experimental data. Over certain ranges of molecular weight M and shear rates γ, power laws were established early in rheological measurements[1] and also for local and global conformational properties of chains as measured in birefringence and scattering experiments. They are associated with scaling behavior, which plays a central role in the understanding and characterization of linear polymers in dilute solution in equilibrium as well as in nonequilibrium situations.[7,8] The power laws define characteristic (scaling) exponents and enable descriptions of structural and rheological properties of polymer systems by "master" plots, which indicate the underlying self-similarity of the polymer system and, more often, of the polymer chain itself.[7,8] The theoretical foundations of static and dynamic scaling in polymer solutions based on renormalization group methods were established by de Gennes[8,9] and are further discussed by des Cloizeaux.[10] Since the static scaling is connected with spatial correlation lengths, dynamic scaling is based on hydrodynamic length scales.

For more than 25 years, nonequilibrium molecular dynamics (NEMD) has provided a powerful supplement to experimental and analytical techniques.[11] Molecular dynamics studies offer insight into the dynamics of polymers, since they naturally connect the conformational properties of polymer chains with macroscopic properties. In previous MD simulations various model systems have been used to study polymer melts and solutions in equilibrium (bead−FENE−spring chains),[12−14] polymer solutions in equilibrium and under shear flow (bead−rod chains),[15,16] polymer solutions under shear flow (Lennard-Jones-chains),[17] and polymer melts under shear and elongational flow.[18]

This article is devoted to extensive NEMD studies of a plane Couette flow of dilute polymer solutions containing FENE chains of various lengths N. Over a great range of shear rates results are obtained for the flow-induced anisotropy of the pressure tensor, the alignment tensor, the gyration tensor, the end-to-end tensor, and the static structure factor. The NEMD results are also expressed in terms of power laws, the exponents and

* Corresponding author. E-mail: aust@physik.tu-berlin.de.
† Technische Universität Berlin.
‡ The Hebrew University.
§ ETH Zürich.

10.1021/ma981683u CCC: $18.00
Published on Web 07/30/1999

prefactors of which are compared with analytic theories and experimental data. Furthermore the rotation of a whole chain in the Couette flow field is analyzed. Firstly, however, the equilibrium molecular structure and diffusion are investigated. The specific microscopic model chosen corresponds to that of Dünweg and Kremer, who have performed extensive equilibrium molecular dynamics studies.[13,14]

Theoretical predictions for the behavior of macromolecular solutions subjected to shear flow have been given for simple polymer models using Gaussian chains (GC), Rouse chains (RC), FENE chains, or wormlike chains.[1,7,10,19] However, the analytical approach requires additional simplifications, and for all previous calculations one or more of the following features were neglected or roughly approximated: hydrodynamic interaction (HI), excluded volume (EV), and finite extendability. Moreover, reliable predictions are often restricted to the linear flow regime. Unlike the GC or RC models, the FENE model is a promising candidate to describe the rheo-optical behavior of real polymer solutions, since its inherent nature of finite extendability closely resembles the local characteristics of real polymer chains on a coarse-grained level.[1] In addition to the nonequilibrium molecular dynamics (NEMD) method, which, in our case, treats the hydrodynamic interactions (HI) by considering the solvent particles explicitly, nonequilibrium Brownian dynamics methods became popular to study polymer solutions, since, in comparison with molecular dynamics, it is for chains of small and intermediate lengths a computationally less time-consuming method.[19−22] Interrelations between the two methods, when applied to similar model polymer solutions, will be discussed.

Experimental data obtained from sheared polymer solutions and containing rheological or structural information are usually plotted versus a dimensionless shear rate, β, which is the product of the shear rate and a relaxation time, as usually determined from the intrinsic viscosity. For any polymer solution, such relaxation times can be estimated; they are often regarded as dominating not only the rheology but also the underlying microscopic process. The range of experimentally accessible shear rates for laminar flows is limited to approximately $0.2 < \beta < 40$, due to the signal-to-noise ratio (lower limit) and the occurrence of flow instabilities (upper limit). Here, in the simulations, data are presented for reduced shear rates in the range 0.2−1000.

This article is organized as follows: In section 2 the simulation model system is described. Section 3 is devoted to the phenomenological framework of a polymer chain subjected to shear flow and the method of analyzing our simulation data for chains with different molecular weights (contour lengths). The analysis concentrates on scaling rules, the determination of relaxation times, and master plots. The results are presented and discussed in section 4 and ordered into discussions about equilibrium properties, rheological data, flow-induced alignment, deformation of chains, static structure factors, and the rotational dynamics of chains. A summary and conclusions are given in section 5.

2. Model and Simulation Technique

In this work, the nonequilibrium properties of a microscopic model system for a dilute polymer solution under good solvent conditions have been simulated. The system consists of a single linear chain of $N = 10$, 20, 30, or 60 beads dissolved in a bath of N_s solvent particles. Following from our (freely chosen) constraint $n = N/N_t \approx 1\%$, the total number of particles, $N_t = N + N_s$, ranges between $N_t = 1000$ and 5832.

All particles are of identical mass, m, and the pair interaction between all particles is modeled by a purely repulsive Lennard−Jones potential (WCA).[23]

$$U^{\mathrm{WCA}}(r) = \begin{cases} 4\epsilon\left(\left(\frac{\sigma}{r}\right)^{12} - \left(\frac{\sigma}{r}\right)^{6} + \frac{1}{4}\right) & r \le r_c \\ 0 & r > r_c \end{cases} \qquad (1)$$

In eq 1, r denotes the spatial distance between particles and $r_c = 2^{1/6}\sigma$ is the cutoff radius. The energy and length parameters of the WCA−Lennard−Jones potential ϵ and σ and the particle mass m fix a unit system by which all relevant quantities are expressed throughout the paper; e.g., reference units for time, density, temperature, and pressure are $t_{\mathrm{ref}} = \sqrt{m\sigma^2/\epsilon}$, $\rho_{\mathrm{ref}} = \sigma^{-3}$, $T_{\mathrm{ref}} = \epsilon/k_B$, and $p_{\mathrm{ref}} = \epsilon\sigma^{-3}$, where k_B denotes the Boltzmann constant. The simulations were performed in a volume V at a state point with particle number density $\rho = N_t/V = 0.864$ and temperature $T = 1.2$. The thermomechanical properties of the WCA−Lennard−Jones model system in both its fluid and solid states are discussed in ref 24.

The formation of a linear polymer chain requires a connectivity between beads, which is achieved by connecting N neighboring pairs of the N_t particles through the addition of an attractive interaction potential, U^{FENE}, introduced by Warner[25]

$$U^{\mathrm{FENE}}(r) = -\frac{k}{2}R_0^{\,2}\ln\left(1 - \frac{r^2}{R_0^{\,2}}\right) \qquad (2)$$

with parameters $k = 7$ and $R_0 = 2$. The FENE parameters and also the state point (particle number density/temperature as above) were chosen in accordance with previous works of Dünweg and Kremer, who studied similar systems in their equilibrium states.[13,14] Despite the FENE potential along the chain segments, there are no differences between solvent particles and chain monomers, i.e., the solvent is ideally good (athermal). Note that each model segment corresponds to a number of real bonds (typically 3−7), which depends on the actual chemistry, i.e. the chains persistence length.[26]

All particles are located within a rectangular simulation cell ($V = N_t/\rho = L_xL_yL_z$). In order to study bulk properties, the method of periodic images has been implemented. In general, we use noncubic simulation cells which are stretched (values are given in Table 1) in flow direction in order to avoid self-interactions of the polymer chain with its periodic images. The flow is imposed by applying the Lees−Edwards boundary conditions.[27]

In order to start the simulation, all particles were placed on a simple cubic lattice. The particles belonging to the polymer chain are chosen on the basis of a self-avoiding random walk procedure. The initial velocities were chosen from a Maxwellian distribution. Newton's equations of motion were integrated by a velocity−Verlet algorithm with an integration time step $\Delta t = 0.005$ for shear rates $\gamma < 0.6$ and $\Delta t = 0.003/\gamma$ for $\gamma \ge 0.6$. We averaged the final data over 5×10^3 and 4×10^4 time units t_{ref} at high and low shear rates, respectively. The first 20% of these runs are discarded in the analysis, in order to eliminate any influence of the initial

conditions. The temperature was kept constant (NVT ensemble) by rescaling the magnitude of the particle peculiar velocities, which corresponds to the Gaussian constraint of constant kinetic energy.[28]

We studied the effect of shear flow and chain length N, where the shear rate γ was varied over a range of about four decades up to $\gamma = 3$. Above this shear rate the polymer chains tend to break, due to numerical instabilities at reasonable integration time steps. The lower limit is determined by the unfavorable signal-to-noise ratio at low shear rates, since close to equilibrium most shear-induced perturbations evaluated here are linear or quadratic functions of γ. For the lowest shear rate, no significant deviations from the equilibrium results as obtained earlier by Dünweg and Kremer[14] were found. To achieve an accurate evaluation of scaling exponents, which requires a variation of N by a factor of at least 3, and to keep the needed CPU time ($\approx 10^{-5}$ s per particle and integration time step) reasonable, we had to perform our calculations for rather short chains with $N \leq 60$.

3. Phenomenological Framework and Evaluation of Data

The systems under study are anisotropic in nature as a result of the imposed shear flow fields. Specifically, the flow velocity field has the form $\mathbf{v} = (\gamma y, 0, 0)$ with shear rate γ, which fixes the following specifications: flow (x), gradient (y), and vorticity (z) direction. Shear-induced deviations from the equilibrium behavior are measured by tensorial quantities, i.e., the pressure tensor, $\mathbf{P}$; the intrinsic pressure tensor, $\mathbf{P}^{\text{int}}$; the tensor of gyration, $\mathbf{G}$; the end-to-end tensor, $\mathbf{R}$, and the alignment tensor, $\mathbf{A}$, which are all defined in section 4. For symmetry reasons, the statistical average of any (3 $\times$ 3) symmetric tensorial quantity $\mathbf{X}$ in this coordinate system involves only four variables, since its xz, zx, yz, zy components vanish. Moreover, for traceless tensorial quantities only three independent nonzero components remain. In equilibrium ($\gamma = 0$), all tensorial quantities are reduced to their scalar, or isotropic, counterparts.

According to theoretical predictions, the shear-induced perturbations of various components of tensorial quantities $\mathbf{X}$ are linear or quadratic functions of shear rate. For instance a Newtonian rheology requires $P_{xy} \propto \gamma$. Even if these predictions tend to fail at high shear rates, one may expect the power-law behavior to hold in the weak flow regime, a fact which is confirmed experimentally in many cases.[1] As a consequence for all extracted tensorial quantities, close to equilibrium the shear-induced deviations from equilibrium values are of the same order as their error bars. The unfavorable signal-to-noise ratio limits the useful applicable range of shear rates not only in NEMD but also in experiments. For example, in light-scattering experiments the measured intensity is only slightly dependent on the scattering angle, which shows a rather broad maximum used to estimate the orientation angle.[5,29,30]

Deformation and Orientation of the Polymer Coil. The deformation of the polymer coil (and of any subpart of the polymer coil, e.g., of a polymer segment) can be measured both relative to a laboratory-fixed coordinate system, e.g., via the diagonal elements of the tensor of gyration, and relative to a molecule-fixed coordinate system (via its eigenvalues). Let the eigenvalues of the tensorial quantity $\mathbf{X}$ be ordered and denoted by X_A (largest), X_C, and X_B (smallest eigenvalue). The corresponding main axes A, B span the shear (xy) plane, and C is parallel to the vorticity (z) direction.

The degree of alignment of a tensor which represents the orientation of a (subpart of a) polymer chain can be quantified by the flow-alignment angle, χ_X, via

$$\cot(2\chi_X) = \frac{X_{xx} - X_{yy}}{2X_{xy}} \equiv \frac{\beta}{m_X} \tag{3}$$

where m_X behaves as an orientational resistance parameter. This value gives the angle between the main axis A and the flow (x) direction. Close to equilibrium, i.e., for low shear rates, one typically finds $X_{xy} \propto \gamma$ and $(X_{xx} - X_{yy}) \propto \gamma^2$, hence m_X is independent of γ and $\chi_X \approx 45°$. For the polymer coil, e.g., when $\mathbf{X}$ denotes the tensor of gyration or the end-to-end tensor, the onset of a decrease of χ_X with shear rate γ appears at a dimensionless shear rate $\tau\gamma^* = 1$, thus defining a relaxation time τ and a characteristic shear rate γ^*. The computation of γ^* or τ from the simulation data is described explicitly below.

Evaluation and Interpretation of Specific Simulation Data. As mentioned before, commonly a single relaxation time τ is used to define a dimensionless shear rate $\beta \equiv \tau\gamma$. Accordingly, all measured or calculated quantities are plotted versus β with the assumption that characteristic shear-induced changes take place at the same value of β for chains of different lengths N or molecular weight M. From our simulation data it is possible to test this assumption by specifying characteristic shear rates for all but a few measured quantities (from a single system and measured simultaneously) independently. Therefore different relaxation times will be involved, even for a fixed chain length. For the sake of clarity, the dimensionless shear rate will appear with an index which specifies the property used to determine the corresponding relaxation time, i.e. $\beta \rightarrow \beta_{\chi X} \equiv \tau_{\chi X}\gamma$ in eq 3.

In general, for any $\beta_X \ll 1$ the related quantity X approaches its equilibrium value X_0 and for $\beta_X \gg 1$ we find $X \propto \beta_X^{\mu}$ with a characteristic exponent μ over a wide range of shear rates. Such relationships do occur frequently in the field of polymer rheology representing Newtonian flow behavior $\eta = \eta_0$ at low shear rates and the power law $\eta \propto |\gamma|^{q-1}$ of Ostwald and de Waele at high shear rates.[31] The exponent q describes the strength of shear-induced changes; for instance, if X denotes the shear viscosity η, shear "thinning" and "thickening" are represented as $q < 1$ and $q > 1$, respectively.

In this work we fit our data to an interpolation formula for both relations

$$X(\gamma) = X_0 [1 + |\tau_X\gamma|^{\kappa}]^{\mu/\kappa} \tag{4}$$

wherein the parameter τ_X has the dimension of time and the slope of X at high $\beta_X \equiv \tau_X\gamma$ values (in the non-Newtonian regime) is determined by μ. Equation 4 is closely related to the Yasuda function in the case of $X_\infty \equiv \lim_{\gamma\rightarrow\infty} X(\gamma) = 0$.[1,32] Unlike the well-known Carreau equation the function 4 contains an additional parameter, κ, which determines the width of the crossover region at $\beta_X = 1$. With increasing κ, i.e., when the kink between the limiting relations becomes rather smooth, an accurate calculation of τ_X becomes difficult.

When the simulation data of various quantities X are fitted to eq 4, the values X_0, τ_X, and their specific dependencies on the chain length N are analyzed in terms of power laws

$$X_0 \equiv aN^{\nu} \quad \text{and} \quad \tau_X \equiv bN^{\alpha} \tag{5}$$

thus providing values for a, ν, b, and α. These dependencies are then compared to the experimentally known and theoretically predicted relationships. Whenever the exponent μ is (found to be) independent of chain length N, the functions defined in eq 4 can be transformed in order to be plotted on a master plot by applying the following transformation rule $X \rightarrow F_X$ with

$$F_X(\beta_X = \tau_X\gamma) = \frac{X(\tau_X\gamma)}{X_0} = \frac{X(bN^{\alpha}\gamma)}{aN^{\nu}} \tag{6}$$

As required for a master curve, F_X is thus independent of the chain length N.

4. Results and Discussion

A. Equilibrium Properties and Behavior Close to Equilibrium. In order to quantify the shear-induced structural changes of the system, we have to characterize it in the equilibrium state. Instead of analyzing fluctuations and correlation functions for $\gamma = 0$,[33,34] we performed simulations at small shear rates and extrapolate our data in the limit of $\gamma \rightarrow 0$. Whenever possible the results are compared with those of Dünweg and Kremer.[14]

Solvent and Intrinsic Viscosity. The shear viscosity of the polymer solution $\eta = -P_{yx}/\gamma$ is calculated from the pressure tensor $\mathbf{P}$, which is obtained via the tensor version of the virial theorem[28]

$$\mathbf{P} = \frac{1}{V}\left\langle \sum_{i}^{N_t} (\mathbf{c}_i\mathbf{c}_i + \sum_{j<i}^{N_t} \mathbf{F}_{ij}\mathbf{r}_{ij}) \right\rangle \tag{7}$$

with the coordinates $\mathbf{r}_i$ and $\mathbf{r}_{ij} = \mathbf{r}_j - \mathbf{r}_i$, the forces $\mathbf{F}_{ij} = \mathbf{F}(\mathbf{r}_{ij})$, and the peculiar velocities $\mathbf{c}_i = \mathbf{v}_i - \mathbf{v}(\mathbf{r}_i)$. In the equilibrium limit $\gamma \rightarrow 0$, we obtain $\eta[N] \approx \eta^s = 2.4 \pm 0.1$ in good agreement with ref 14. No influence of the chain length N was observable within the statistical error.

The intrinsic viscosity $[\eta]_0$ specifies the influence of a polymer chain on the viscosity of the polymer solution η in the limit of an infinitely dilute solution close to equilibrium. One defines[35,36]

$$[\eta]_0 = \lim_{\gamma\rightarrow 0} \lim_{c\rightarrow 0} \frac{\eta - \eta^s}{c\eta^s} \tag{8}$$

where $c = N/V$ and η^s denote the mass concentration of polymer beads and the viscosity of the solvent, respectively. Often $[\eta]_0$ is used to estimate the longest relaxation time

$$\tau = \frac{\eta^s[\eta]_0}{k_BT} M \propto M^a M \propto N^{1+a} \tag{9}$$

Here a is the Mark−Houwink exponent, which determines the dependence of τ and $[\eta]_0$ on the chain length (or molecular weight M), and it "measures" the solvent quality.

By means of molecular dynamics it is rather difficult to determine this limit according eq 8 with sufficient accuracy, since for small concentrations the statistical errors of η and η^s are on the order $\eta - \eta^s$. Splitting the stress tensor $\mathbf{P}$ into two parts, where one part stems directly from the chain−chain interactions, allows values for the intrinsic (intramolecular) rheological functions by the MD simulation to be estimated. The intrinsic stress tensor $\mathbf{P}^{int}$ we extract here is defined by

$$\mathbf{P}^{int} \equiv \frac{1}{n\eta^s}\frac{1}{2V}\left\langle \sum_{i,j}^{N} \mathbf{r}_{ij}\mathbf{F}_{ij}^{FENE} \right\rangle \tag{10}$$

since we assume $n\eta^s\mathbf{P}^{int} \approx \mathbf{P} - \mathbf{P}^s$. Here $n = N/N_t = c\rho$ is the monomer density, $\mathbf{P}^s$ is the stress tensor of the pure solvent, $\mathbf{F}_{ij}^{FENE}$ is the FENE force acting between particle i and j, and $\langle ... \rangle$ indicates a statistical average.

Using this formula for the intrinsic stress tensor, we calculate the intrinsic viscosity η^{int} and the viscometric functions Ψ_1^{int} and Ψ_2^{int} from its components.[1,17] For the intrinsic shear viscosities $\eta^{int}[N]$ as function of N the extrapolated values are $\eta_0^{int}[N] = 3.8 \pm 0.4$, 7.4 ± 0.7, 11.3 ± 1.0, and 23 ± 3 for $N = 10$, 20, 30, 60, yielding $\eta_0^{int} = 0.39N^a$ with a Mark−Houwink coefficient $a = 1.0 \pm 0.1$, which has to be compared with experimental findings ($a = 0.70-0.75$)[37] and theoretical predictions ($a = 0.764-0.8$)[10,38] for good solvents. The differences seem to stem from the fact that there is no one-to-one relationship between the experimentally measured intrinsic stress tensor and our construction of an intrinsic stress tensor, which favors a value of $a \approx 1$. This, however, will not effect the analysis of the other quantities studied below.

Conformational Properties. The conformational anisotropy of a polymer coil under shear, i.e. its deformation and orientation, can be quantified by various tensorial quantities such as the end-to-end tensor $\mathbf{R}$ and the gyration tensor $\mathbf{G}$. For a chain consisting of N beads with coordinates $\mathbf{r}_i$ and $\mathbf{r}_{ij} = \mathbf{r}_j - \mathbf{r}_i$, these tensors are defined as

$$\mathbf{G} \equiv \frac{1}{2N^2}\sum_{i,j}^{N} \langle \mathbf{r}_{ij}\mathbf{r}_{ij} \rangle \tag{11}$$

$$\mathbf{R} \equiv \langle (\mathbf{r}_N - \mathbf{r}_1)(\mathbf{r}_N - \mathbf{r}_1) \rangle \tag{12}$$

The mean squared radius of gyration, r_G, and the mean squared end-to-end distance r_R are obtained from the trace of the corresponding tensors, i.e., $r_G^2 = \mathrm{Tr}\ \mathbf{G}$ and $r_R^2 = \mathrm{Tr}\ \mathbf{R}$.

The simulation results for the equilibrium values of the radii of gyration and the end-to-end distances are $r_G[N] = 1.64 \pm 0.04$, 2.48 ± 0.05, 3.18 ± 0.06, and 4.79 ± 0.08, and $r_R[N] = 4.0 \pm 0.1$, 6.2 ± 0.2, 7.9 ± 0.2, and 12.0 ± 0.3 both for $N = 10$, 20, 30, 60, respectively. They are in good agreement with results of previous MD simulations.[14]

The effect of chain length N on the end-to-end distance and radius of gyration is expressed as $r_R = a_R(N-1)^{\nu}$ and $r_G = a_G[(N^2-1)/N]^{\nu}$, respectively, where ν is referred to as a static scaling exponent. In the limit of large N, the latter relationship is reduced to $r_G \propto N^{\nu}$. From the simulation we obtain $a_G = 0.419 \pm 0.003$, $\nu = 0.595 \pm 0.002$, and $a_R = 1.096 \pm 0.011$, $\nu = 0.587 \pm 0.002$. These values for the exponent are close to $\nu =$

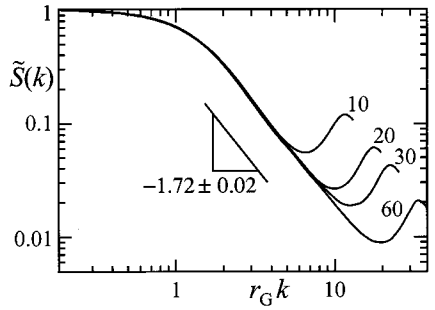

Figure 1. MD data. The normalized equilibrium static structure factor $\tilde{S}(k) = S(k)/S(0)$ versus $r_G k$ for various chain lengths. The figure shows the universal behavior $S(k) \propto k^{-1/\nu}$, valid for $2 \leq r_G k < 4r_G$ with $\nu = 0.583 \pm 0.008$.

0.588, as expected from renormalization group theory[10] and to $\nu = 0.6$, as predicted by Flory.[39] The stated formulas work well even for short chains and even dumbbells ($N = 2$) for which $r_R^2/r_G^2 = 4$ by definition. The averaged mean squared bond length

$$s^2 = \frac{1}{N-1}\left\langle \sum_{i=1}^{N-1} |\mathbf{r}_{i+1} - \mathbf{r}_i|^2 \right\rangle = 1.130 \pm 0.012 \quad (13)$$

is found to be independent of the chain length in the weak flow regime. Hence the values for dumbbells are $r_G[2] = 0.531 \pm 0.004$ and $r_R[2] = 1.063 \pm 0.008$, which is very close to $r_G[2] = 0.533 \pm 0.003$ and $r_R[2] = 1.096 \pm 0.011$ as it follows from the power "laws". For the squared ratio between end-to-end distance and radius of gyration, the simulation yields $r_R^2/r_G^2 = 6.2 \pm 0.1$, as expected for a self-avoiding random walk and also for a polymer chain subjected to good solvent conditions.[10]

Static Structure Factor. The deformation and orientation of both the whole chain and the local structure is measured by analyzing the single chain static structure factor

$$S(\mathbf{k}) = \frac{1}{N}\sum_{i,j}^{N} \langle \exp(-i\mathbf{k}\cdot\mathbf{r}_{ij}) \rangle \quad (14)$$

The experimentally measured scattering intensity is connected with the structure factor by multiplying $S(\mathbf{k})$ by a form factor of a Kuhn segment[40] of a real polymer chain. The structure factor for small values of the scalar wave vector transfer $k = |\mathbf{k}| \ll 1/r_G$ is related to the number of scattering units, here the chain length N and the tensor of gyration via

$$S(\mathbf{k}) = N\,(1 - \mathbf{k}\cdot\mathbf{G}\cdot\mathbf{k} + O(k^4)) \quad (15)$$

The intermediate regime ($2.5/r_G < k < 4/s$, with segment length s) contains the information about the intramolecular spatial correlation between particles.

Close to equilibrium the structure factor $S(\mathbf{k}) = S(k)$ of the polymer chain is isotropic and depends only on the magnitude of the scattering wave vector $k \equiv |\mathbf{k}|$. When plotting $S(k)/N$ versus $r_G k$, we obtain for $k < 4/s$ a single line (Figure 1). For larger k values, the N-independent local structure is resolved. Within the intermediate regime, the structure factor decreases according to $S(k) \propto k^{-1/\nu}$, with $\nu = 0.583 \pm 0.008$ being independent of the chain length. This approach provides basically an alternative method to determine ν (in addition to the r_G route). Its value is again close to the theoretical value.

Chain Diffusion Coefficient and Hydrodynamic Radius. The simple bead−spring models of Rouse and Zimm predict a chain length dependence for the longest relaxation time which is given by

$$\tau \propto r_G^2/D \quad (16)$$

where D is the chain diffusion constant, predicted to be $D \propto N^{-1}$ (Rouse) and $D \propto N^{-\nu'}$ (Zimm) with dynamic scaling exponents of $\nu' = 0.5$ and $\nu' = 0.6$ under Θ and good solvent conditions, respectively.[7] In order to compare the results of eq 16 with those obtained from eq 9, we determined the diffusion constant D of the polymer from the autocorrelation function of its center of mass according to

$$D = \lim_{t\to\infty} \frac{1}{6t}\langle (\mathbf{r}_{cm}(t) - \mathbf{r}_{cm}(0))\cdot(\mathbf{r}_{cm}(t) - \mathbf{r}_{cm}(0)) \rangle \quad (17)$$

An alternative method to calculate D is provided by the Kirkwood formula[33]

$$D = \frac{D_0}{N} + \frac{k_B T}{6\pi\eta^s}\frac{1}{r_h} \quad (18)$$

where D_0 denotes the monomer diffusion constant and r_h is the hydrodynamic radius

$$\frac{1}{r_h} = \frac{1}{N^2}\sum_{i\neq j}\left\langle \frac{1}{|\mathbf{r}_{ij}|} \right\rangle \quad (19)$$

Here, r_h stands for the radius of a sphere which possesses the same friction coefficient as the polymer coil. As a result of the long-range nature of hydrodynamic interactions and the influence of periodic image particles, both properties r_h and D depend on the size of the simulation cell. In the case of r_h this becomes quite evident, since there are two ways of defining $\mathbf{r}_{ij}$: (i) from the unfolded chain and (ii) from the absolute coordinates within the central simulation cell. In the following the subscript "$_L$" is used to indicate properties affected by the finite system size. In order to test the applicability of the Kirkwood formula and, taking its validity for granted, to determine D, we have to take finite size effects into account properly. Here we follow the route proposed by Dünweg and Kremer,[14] who incorporated this effect in the Kirkwood−Riseman theory[33] by replacing the Oseen tensor by the corresponding Ewald sum.

According to this scheme we estimated the inverse hydrodynamic radius $r_{h,L}^{-1}[N] = 0.25 \pm 0.02$, 0.204 ± 0.017, 0.168 ± 0.013, and 0.111 ± 0.008 and the chain diffusion constant as measured from the particle displacements $D_L[N] \times 10^2 = 1.47 \pm 0.04$, 0.93 ± 0.03, 0.70 ± 0.02, and 0.43 ± 0.01 for $N = 10$, 20, 30, 60 and the values for L given in Table 1. As previously found,[14] the finite size values are consistent with eq 18, which can be used to determine the N- and L-independent monomer diffusion constant $D_0 = 0.079 \pm 0.003$. The hydrodynamic radii as obtained from the unfolded chain coordinates, i.e., corresponding to the limit $L \to \infty$, are $r_h^{-1}[N] = 0.55 \pm 0.03$, 0.41 ± 0.03, 0.34 ± 0.02, and 0.25 ± 0.02 for $N = 10$, 20, 30, 60 and emphasize the large influence of the system size.

According to the Zimm model with equilibrium-averaged hydrodynamic interaction, the ratio r_G/r_h becomes universal in the long chain limit, i.e., independent of both the chain length N and the hydrodynamic

Table 1. System Sizes: Number of Particles (N), Chain Lengths (N), and Box Lengths ($L_{x,y,z}$) for the Systems under Study

	cubic cell		rectangular cell[a]		
N	N_t	L	N_t	L_x	$L_y = L_z$
10	1000	10	1000	10	10
20	1728	12	2000	20	10
30	2744	14	3000	30	10
60	5832	18	5760	40	12

[a] The shape of the rectangular simulation cells account for the flow-induced shape of the polymer chain at reduced shear rates $\beta_{\chi G} > 3$. The flow direction is parallel to the x axis.

interaction strength, and its value is 1.47934.[19] Our results for the model, which has to be regarded as a specific realization of the hydrodynamic interaction strength for finite chain lengths N, follow the empirical rule $r_G/r_h \approx 1.52 - 2.39/\sqrt{N}$. A numerical study of the universal ratio for the Zimm model without equilibrium-averaged hydrodynamic interaction has still to be carried out.

Taking the Kirkwood−Riseman formula (eq 18) for granted we are now able to calculate the chain diffusion coefficient in the limit of infinite system size, $D[N] \times 10^2 = 2.25 \pm 0.20$, 1.47 ± 0.16, 1.16 ± 0.11, and 0.79 ± 0.07 for $N = 10$, 20, 30, 60, i.e., $D \approx (0.086 \pm 0.005) N^{-\nu'}$ with $\nu' = 0.58 \pm 0.02$, which is close to the static scaling exponent ν. A quite convenient estimate of the corresponding relaxation time $\tau_D = r_G^2/6D$ is based on eq 16 and identifies τ_D with the time a polymer chain needs to be spatially displaced by a distance which is comparable to its own size. We find $\tau_D[N] = 20 \pm 2$, 70 ± 9, 145 ± 15, and 490 ± 50 for $N = 10$, 20, 30, 60, i.e., $\tau_D \propto N^{1.77\pm0.04}$ in quantitative agreement with the Zimm relaxation time $\tau_Z = 4.93\eta^s r_G^3/(\sqrt{6}k_BT)$.[7]

Many analytical theories assume a single characteristic relaxation time, and thus experimental data are often discussed in terms of a single relaxation time for which the crossover from linear to nonlinear behavior sets in at the dimensionless shear rate $\beta = \tau\gamma = 1$. In the following we show to what extent such a treatment is useful if rheo-optical properties have to be discussed.

B. Rheology. The NEMD studies show that for high shear rates ($\gamma \geq 0.5$) both the pure solvent and the polymer solutions display nonlinear rheological behavior, i.e., we observe shear thinning and normal stress differences. At the small concentrations under study, the effect of the dissolved polymers on the solution viscosity is resolved by studying the intrinsic stress tensor, as defined in eq 10.

The shear thinning behavior of the intrinsic viscosity, $\eta^{int} = -P_{xy}^{int}/\gamma$, is much more pronounced than that of the solution viscosity (for example, at $\gamma = 3$, $\eta/\eta_0 \approx 0.7$, independent of N and $\eta^{int}/\eta_0^{int} \approx 1.2/N$). As shown in the upper part of Figure 2, the simulation data of the intrinsic viscosity versus γ can be reproduced by a set of modified Carreau functions (dashed lines). Following eq 4, each of these functions involves two exponents, μ and κ, for which we find $\mu = -0.59 \pm 0.02$ and $\kappa = 3 \pm 1$, independent of chain length. Experimentally, μ ranges from -0.4 to -0.85,[1] whereas most theories predict either $\mu = -2/3$[41−43] or no shear thinning ($\mu = 0$). As already shown for η_0^{int}, τ_η scales with N as $\tau_\eta = (0.53 \pm 0.02)N^{3\nu'}$ with $\nu' = 0.54 \pm 0.02$. More specifically we have $\tau_\eta[N] = 22 \pm 3$, 68 ± 9, 125 ± 15, and 400 ± 40 for $N = 10$, 20, 30, 60. These values for the relaxation times are close to those we obtained for τ_D above. In order to obtain a single N-independent master plot, we insert the power laws for η_0^{int} and τ_η in eq 6. The result is shown in the lower part of Figure 2 and confirms the scaling picture proposed in section 3.

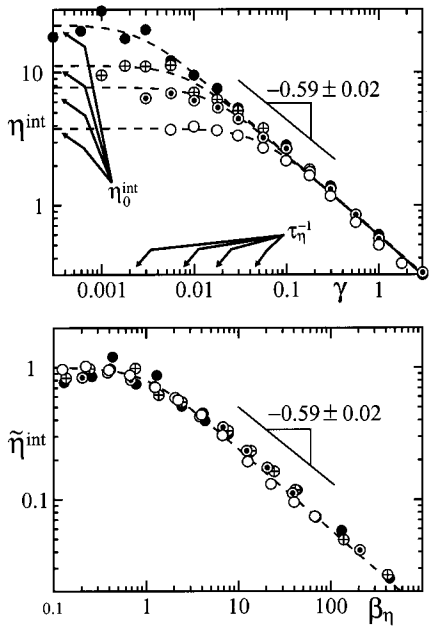

Figure 2. From the plotted data for the intrinsic viscosity η^{int} versus shear rate γ, the zero rate shear viscosities $\eta_0^{int}[N]$, and the relaxation times $\tau_\eta[N]$ for various chain lengths N are determined by fitting these data to modified Carreau functions (dashed curves, see section 3 and eq 4). The circles specify the chain lengths $N = 10$ (open), $N = 20$ (pointed), $N = 30$ (crossed), and $N = 60$ (filled). In the strong flow regime the strength of shear thinning $\mu = -0.59 \pm 0.02$ is independent of the chain length. When $\tilde{\eta}^{int} = \eta^{int}/\eta_0^{int}$ versus the reduced shear rate $\beta_\eta = \tau_\eta\gamma$ is plotted, a "master" plot is obtained (details are given in section 3).

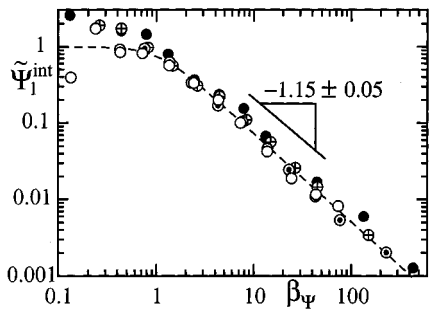

Figure 3. The reduced first viscometric function $\Psi_1^{int} = \Psi_1^{int}/\Psi_{10}^{int}$ versus the reduced shear rate $\beta_\Psi = \tau_\Psi\gamma$ according method II for various chain lengths (same symbols as in Figure 2). These functions are well approximated by a modified Carreau function with an exponent of $\mu = -1.15 \pm 0.05$.

In comparison with the shear viscosity, normal stress differences are more difficult to measure, not only in experiments but also from computer simulations. The intrinsic first viscometric function Ψ_1^{int} is larger than zero, and within a wide range of shear rates, we find $\Psi_1^{int} \propto \gamma^{-1.15\pm0.05}$, independent of N (Figure 3). Analytical theories lead to a slightly stronger shear rate dependence ($\mu = -4/3$),[41−43] provided that they predict non-Newtonian rheology. For the first viscometric function, the simple extrapolation scheme ("method I") yields $\Psi_{10}^{int} \propto N^{3.0\pm0.4}$ and $\tau_\Psi \propto N^{1.9\pm0.3}$. We obtain a more precise value for the viscometric function by extrapolating the shear modulus $G = (2\eta^{int})^2/\Psi_1^{int}$ to low shear

Table 2. NEMD Data for the Shear-Induced Intrinsic Shear Viscosity (η^{int}), the Radius of Gyration (r_G), the Flow-Alignment Angle of the Radius of Gyration (χ_G) and of the Polymer Segments (χ_A), the Orientational Resistance Parameter (m_G), and the Reduced Angular Velocity of the Polymer Coil ($-\omega_z/\gamma$)

γ^a	β_D	η^{int}	r_G	χ_G	χ_A	m_G	$-\omega_z/\gamma$
			$N = 10$				
0.01	0.2	3.92	1.63	36	38.4	1.1	0.4
0.03	0.6	3.33	1.65	30.5	34.7	1.9	0.54
0.1	2.0	2.17	1.77	16.6	25.9	2.3	0.34
0.3	6.0	1.17	2.00	10.3	18.0	4.0	0.21
1.0	20	0.50	2.2	6.7	12.5	8.3	0.114
3.0	60	0.29	2.9	2.9	5.1	10.8	0.042
			$N = 30$				
0.001	0.15	10.4	3.24	31.0	30	0.6	0.6
0.003	0.44	11.1	3.30	24.6	33	1.1	0.47
0.01	1.5	7.08	3.67	16.8	26.4	2.2	0.26
0.03	4.4	5.38	4.32	11.0	19.7	4.0	0.21
0.1	15	2.79	5.51	6.5	13.7	7.6	0.092
0.3	44	1.38	6.94	4.1	8.7	14.2	0.032
1.0	150	0.58	8.49	1.74	5.7	20	0.017
3.0	440	0.29	9.22	0.71	3.6	46	0.009
			$N = 60$				
0.0003	0.15	22.8	4.78		31		0.4
0.001	0.49	21.2	5.40	28	36	2.0	0.50
0.003	1.5	20.4	5.87	20.5	27.7	3.5	0.40
0.01	4.9	9.82	6.75	9.1	16.9	4.4	0.23
0.03	15	5.00	10.0	4.7	11.1	6.6	0.060
0.1	49	2.84	12.0	4.1	8.3	15.5	0.027
0.3	150	1.40	17.6	1.47	4.9	20	0.008
1.0	490	0.61	19.2	0.67	3.9	31	0.006

[a] The applied shear rate γ (in reduced LJ units) is related to the dimensionless shear parameter β via $\beta_D = \tau_D\gamma$ (see Table 4 for details).

rates ("method II"). This procedure yields $G_0 \propto N^{-0.7\pm0.1}$ and is more easy to apply, since we find that G is independent of γ at low and intermediate shear rates, but decreases slightly with chain length. This method gives $\Psi_{10}^{int} \propto N^{2.7\pm0.2}$ and $\tau_\Psi \propto N^{1.6\pm0.2}$, suggesting $\tau_\Psi = \tau_\eta$. The latter values are used for the N-independent master curve shown in Figure 3.

Since the second viscometric function turned out to be even more difficult to estimate, we were unable to obtain data for $\gamma < 0.03$ with sufficient accuracy. For high rates the second viscometric function takes negative values, and approximately, we find $\Psi_2^{int}/\Psi_1^{int} \propto -1/N$. The signs are expected according to a shear-induced compression of the chain in the direction of the velocity gradient.

C. Orientation and Deformation Phenomena. A detailed analysis of the orientational and deformational properties of the chain subjected to shear flow is presented next. The Tables 2 and 3 contain simulation data of conformational quantities as a function of the chain length N and the shear rate γ. In the following results for the shear-induced local and global anisotropy of the chain will be discussed separately through the (i) alignment and (ii) gyration tensors, respectively.

(i) Alignment Tensor. Stress−Optical Rule. Rheological and flow birefringence measurements in polymeric liquids have shown the wide range of validity of the linear stress−optical rule. This rule claims that the deviatoric components of the stress tensor are proportional to those of the refractive index tensor. It turns out to hold not only for polymer melts[44] but also for polymer solutions if form birefringence can be neglected.[2,45]

Following Kuhn's argument, we assume a linear relationship between the anisotropic part of the refractive index tensor and the alignment tensor **A** defined in eq 20,[46]

Table 3. NEMD Data for the Eigenvalues $G_{A,B,C}$ (see section 4) of the Tensor of Gyration and Its Scaling Exponents $\nu_{A,B,C}$ for a Polymer Solution Subjected to Shear Flow at Various Dimensionless Shear Rates $\beta_D = \tau_D\gamma$ (compare to Table 2)

γ	β_D	G_A	G_B	G_C	ν_A	ν_B	ν_C
			$N = 10$				
0.01	0.2	1.01	0.743	0.907	0.604	0.553	0.578
0.03	0.6	1.30	0.612	0.803	0.631	0.530	0.572
0.1	2.0	1.95	0.472	0.703	0.674	0.526	0.567
0.3	6.0	2.96	0.312	0.728	0.696	0.492	0.594
1.0	20	4.06	0.212	0.429	0.643	0.561	0.643
3.0	60	8.18	0.106	0.348	0.603	0.679	0.676
			$N = 30$				
0.001	0.15	4.18	2.75	2.75	0.597	0.574	0.591
0.003	0.44	4.72	2.71	3.47	0.627	0.537	0.578
0.01	1.5	8.64	2.16	2.71	0.656	0.518	0.557
0.03	4.4	14.7	1.51	2.5	0.714	0.492	0.565
0.1	15	28.0	0.832	1.57	0.731	0.495	0.573
0.3	44	46.6	0.535	0.91	0.727	0.533	0.593
1.0	150	70.8	0.333	0.76	0.689	0.618	0.634
			$N = 60$				
0.0003	0.15	9.82	7.03	6.01	0.592	0.572	0.580
0.001	0.49	18.0	3.79	7.36	0.636	0.538	0.572
0.003	1.5	26.8	4.66	6.78	0.661	0.513	0.556
0.01	4.9	48.2	3.66	4.23	0.707	0.501	0.565
0.03	15	93	1.8	2.65	0.750	0.482	0.553
0.1	49	141	1.29	2.30	0.777	0.518	0.561
0.3	150	309	0.701	1.87	0.736	0.548	0.602

$$\mathbf{A} \equiv \sum_{i=1}^{N-1}\left\langle \mathbf{u}_i\mathbf{u}_i - \frac{1}{3}\mathbf{1}\right\rangle \qquad \mathbf{u}_i \equiv \frac{\mathbf{r}_{i+1}-\mathbf{r}_i}{|\mathbf{r}_{i+1}-\mathbf{r}_i|} \tag{20}$$

where $\langle ... \rangle$ indicates an ensemble or time average. The quantity **A** describes the average orientation of bond segments within the chain, whereas **R** and **G** provide information on the polymer coil. Notice, that **A** corresponds to the alignment tensor which was used in ref 16. Usually, the alignment tensor **a** is defined as $\mathbf{a} = \mathbf{A}/(N-1)$.[47]

Taking Kuhn's approximations for granted, one can write the stress−optical rule as $\mathbf{a} = C_{so}\overline{\mathbf{P}^{int}}$, where $\overline{\mathbf{P}^{int}} = \mathbf{P}^{int} - 1/3(\mathrm{Tr}\ \mathbf{P}^{int})\ \mathbf{1}$ is the anisotropic part of the intrinsic stress tensor. The coefficient of proportionality between the corresponding components of the alignment and stress tensor is called the stress−optical coefficient, C_{so}.

Under special assumptions, i.e., a harmonic bond potential and Gaussian chain statistics, some polymer models predict the stress−optical rule to be exact.[1] But in contrast to the models of Rouse and Zimm, we are using a nonlinear model potential (with its minimum at $r \approx 1.05$) such that the validity of the stress−optical rule is guaranteed only close to equilibrium and at sufficiently low temperatures. This is confirmed by the simulation data, since we find $C_{so} = 0.24 \pm 0.01$ to be independent of N and γ at small and intermediate shear rates, whereas at high shear rates the stress−optical rule is violated and C_{so} decreases for all chain lengths considered.

This is shown in Figure 4, where we present both $A_\eta \equiv A_{xy}/\gamma$ and the intrinsic viscosity η^{int} versus the reduced shear rate β_η. According to its definition, A_{xy} is limited in value and its maximum is found at $\tilde{\gamma} \approx 0.1/N$, whereas $-P_{xy}^{int}$ is a monotonical increasing function of the shear rate. Both curves start to deviate from each other at $\gamma \approx 0.3\ \tilde{\gamma}$, i.e., at $\beta_\eta \approx 1.6N^{0.6} \gg 1$. Hence, the

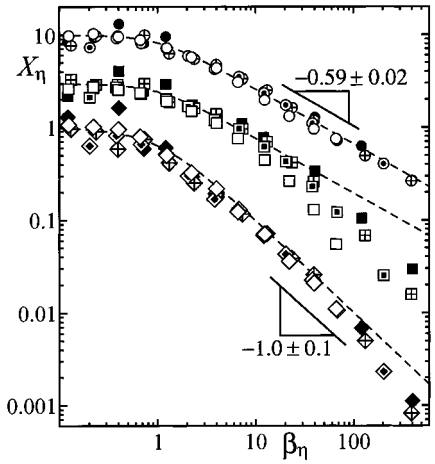

Figure 4. Master plots of $X_\eta = X_{xy}/\gamma$ versus β_η, $= \tau_\eta\gamma$ in arbitrary units for various tensorial properties $\mathbf{X} = \mathbf{P}^{\text{int}}$ (circles), **A** (squares), and **G** (diamonds). The same symbols as in Figure 2 have been used to denote different chain lengths. The prefactors are $10\eta_0^{\text{int}}$, $3A_{\eta 0}$, and $G_{\eta 0}$, respectively (see Table 4).

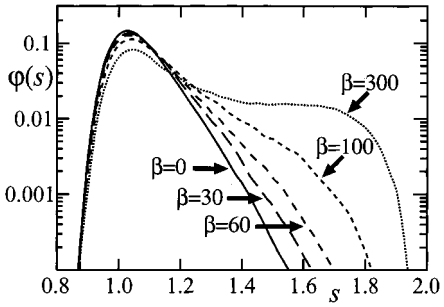

Figure 5. The normalized distribution of segment lengths $\varphi(s)$ versus segment length s for various shear rates and for $N = 30$. In the strong flow regime ($\beta_\eta \geq 30$) bond stretching is pronounced, whereas in the weak and intermediate flow regimes ($\beta_\eta \leq 10$) stretching is below our resolution limit. Close to equilibrium the distribution obeys $\varphi(s) \propto \exp\{-[U^{\text{FENE}}(s) + U^{\text{WCA}}(s)]/k_BT\}$.

corresponding relaxation times for both quantities, η^{int} and A_η, are almost identical. One reason for the deviation at high shear rates is the nonlinearity of the FENE potential, since stretching of segments affects the stress tensor but not the alignment tensor, which is based on the normalized vectors (see eq 20).

Bond stretching is significantly enhanced with increasing shear rate and leads to a decrease of the stress−optical coefficient C_{so}. It is quantitatively connected with the flow-induced shape of the distribution of segment lengths as given in Figure 5 (for $N = 30$). The equilibrium distribution of segment lengths is also plotted in Figure 5. It is well-described by the canonical distribution which involves the Boltzmann factor as well as the model potentials. Whereas, the other curves in Figure 5 measure the tendency of flow-induced segment stretching. At the same time they reflect the shape of the FENE model potential.

Segment Orientation. Despite the above mentioned arguments, the stress−optical rule turns out to be useful even at high shear rates, since the orientation angles for the alignment tensor and for the intrinsic stress tensor coincide. Figure 6 shows the alignment angle χ_A versus reduced shear rate $\beta_{\chi A}$, where we also find a single master curve. In the weak flow regime ($\beta_{\chi A} < 2$), χ_A approaches $\approx 45°$ as predicted theoretically (see

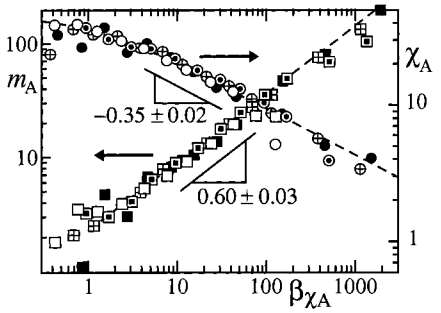

Figure 6. Master plot for the orientation angle χ_A (circles) and the orientation resistance m_A (boxes) versus the reduced shear rate $\beta_{\chi A} = \tau_{\chi A}\gamma$ for various chain lengths (style of symbols as in Figure 2). For shear rates $\beta_{\chi A} \geq 2$ both quantities follow a power law, i.e. $\chi_A \propto \beta_{\chi A}^{-0.35\pm0.02}$ and $m_A \propto \beta_{\chi A}^{0.60\pm0.03}$.

Figure 6). Whereas at high rates, we observe $\chi_A \propto \beta_{\chi A}^{\mu}$ with $\mu = -0.35 \pm 0.02$. For the relaxation times characterizing the behavior of the flow alignment angle we find the following scaling: $\tau_{\chi A} = (0.42 \pm 0.03)N^{2.0\pm0.1}$ ($\tau_{\chi A}[N] = 42 \pm 4$, 168 ± 13, 380 ± 40, and 1470 ± 120 for $N = 10$, 20, 30, 60). This scaling behavior obviously differs significantly from the scaling behavior we detected by analyzing the intrinsic viscosity and the first viscometric function (see Table 4).

Additionally we show in Figure 6 the orientational resistance parameter, m_A, evaluated according to eq 3. In the strong flow regime ($\beta_{\chi A} > 3$), the resistance parameter increases with the shear rate as $m_A \propto \beta_{\chi A}^{0.60\pm0.03}$, in qualitative agreement with previous NEMD simulations.[16] Obviously, with increasing shear rate further orientation of chain segments becomes more difficult. In accordance with the evaluation scheme described in section 3 the strong flow behavior is extrapolated to m_A at $\beta_{\chi A} = 1$, thus approximating the zero-shear rate value m_{A0}, for which we obtain $m_{A0} = 2.4 \pm 0.3$. This behavior serves as a sensitive test of older theories, which predict the resistance parameter to be both independent of shear rate and chain length. For clarity we collect the theoretical predictions of the various models: $m_A = 2.5$ (no hydrodynamic interaction (HI)[48]), $m_A = 4.88$ (pre-averaged HI[38]), $m_A = 3.4 \pm 0.2$ (with HI, Brownian dynamics simulation[21]), or $m_A = 3.28$ (derived from renormalization group studies[49]). Recent birefringence experiments on dilute Θ solutions yield $m_A = 3.0-3.9$ in the weak flow regime.[45] We will continue to discuss this behavior after having presented data for the alignment angle of the gyration tensor.

(ii) Tensor of Gyration and End-to-End Tensor. Roughly, one may expect that the shape of the polymer chain is reflected by the orientation and deformation of its segments. In the following we will show that the orientation and deformation characteristics are coupled to the spatial extension of the bodies.

Chain Orientation. In order to determine the relaxation times connected with the tensor of gyration, we analyze the quantity $G_\eta \equiv G_{xy}/\gamma$. From the results plotted in Figure 4 versus β_η, we find G_η to be constant at low rates; i.e., G_{xy} increases linearly with the shear rate. At high shear rates, G_η decreases according to $G_\eta \propto \gamma^{-1.0\pm0.1}$, since G_{xy} reaches a broad maximum for $\tau_{G\eta}\gamma > 2$. The dashed lines in Figure 4 indicate the Carreau functions used to fit the different quantities. From the present simulations we find the following relaxation times: $\tau_{G\eta}[N] = 23 \pm 3$, 72 ± 8, 130 ± 13, and 400 ± 30 for $N = 10$, 20, 30, 60, i.e., $\tau_{G\eta} = (0.63 \pm 0.09) \cdot N^{1.58\pm0.05}$. For the corresponding quantity R_η, calculated

Table 4. NEMD Data. Summary of the Scaling Behaviors of Relaxation Times τ_X (upper half) and of Rheological and Structural Quantities X_0 (lower half) as Defined and Discussed in the text

	$\tau_X = bN^\alpha$		
τ_X	b	α	corresponding quantity X
τ_η	0.53 ± 0.02	1.62 ± 0.06	shear viscosity η^{int}
τ_Ψ	0.30 ± 0.05	1.9 ± 0.3	first viscometric function Ψ_1 (by method I)
τ_Ψ	0.40 ± 0.05	1.6 ± 0.1	first viscometric function Ψ_1 (by method II)
$\tau_{G\eta}$	0.63 ± 0.09	1.58 ± 0.05	gyration tensor "shear" component G_η
$\tau_{A\eta}$	0.53 ± 0.02	1.62 ± 0.06	alignment tensor "shear" component A_η
$\tau_{\chi G}$	0.85 ± 0.07	2.0 ± 0.1	gyration tensor orientation angle χ_G
$\tau_{\chi A}$	0.42 ± 0.03	2.0 ± 0.1	alignment tensor orientation angle χ_A
τ_ω	0.05 ± 0.01	2.2 ± 0.2	rotation of the polymer chain ω_z
τ_{GA}	0.04 ± 0.02	2.6 ± 0.2	tensor of gyration principal axis A
τ_{GB}	0.7 ± 0.1	1.6 ± 0.1	tensor of gyration principal axis B
τ_{GC}	0.03 ± 0.01	2.0 ± 0.3	tensor of gyration principal axis C
τ_D	0.35 ± 0.02	1.77 ± 0.04	chain diffusion coefficient D
	$X_0 = aN^\nu$		
X_0	a	ν	
η_0^{int}	0.39 ± 0.01	1.0 ± 0.1	shear viscosity η^{int}
Ψ_{10}^{int}	0.3 ± 0.1	3.0 ± 0.4	first viscometric function Ψ_1 (by method I)
Ψ_{10}^{int}	0.11 ± 0.01	2.7 ± 0.1	first viscometric function Ψ_1 (by method II)
r_{R0}	1.096 ± 0.011	0.587 ± 0.002	end-to-end distance r_R ($N \gg 1$)
r_{G0}	0.419 ± 0.003	0.595 ± 0.002	radius of gyration r_G ($N \gg 1$)
D_L	0.070 ± 0.002	-0.69 ± 0.04	chain diffusion coefficient D_L
D	0.086 ± 0.005	-0.58 ± 0.02	chain diffusion coefficient D

from the end-to-end tensor **R** instead of **G**, we observe a rather similar shear rate dependence ($\mu = -1.0 \pm 0.1$ and $\tau_{R\eta} = (0.61 \pm 0.08)N^{1.62\pm0.05}$). These values indicate that the relaxation times for η^{int} and X_η (**X** = **A**, **G** and **R**) follow almost the same power law. This agreement is illustrated in Figure 4, where we present three of these quantities as a function of the *same* dimensionless shear rate β_η.

The simulation results for the orientation angle of the tensor of gyration χ_G are plotted in Figure 7 versus the reduced shear rate $\beta_{\chi G}$ and follow an N-independent master curve (dashed line). For the corresponding relaxation times we find $\tau_{\chi G}[N] = 87 \pm 7$, 340 ± 30, 770 ± 60, and 3000 ± 200 for $N = 10$, 20, 30, 60, i.e., $\tau_{\chi G} = (0.85 \pm 0.07)\ N^{2.0\pm0.1}$. The results approximately obey $\tau_{\chi G} \approx 2\tau_{\chi A}$. At high shear rates, the orientation angle of the polymer coil χ_G decreases faster with flow intensity ($\chi_G \propto \beta_{\chi G}^{\mu}$ and $\mu = -0.45 \pm 0.03$) than the angle of its segments χ_A, for which we find an exponent of $\mu \approx -0.35$. The difference is also visible by comparing the orientational resistance parameters m_G and m_A, as depicted in Figures 7 and 6. Here, for all shear rates we find $m_G < m_A$, i.e., it is easier to align the polymer coil than its segments, independent of the shear rate. (To compare data at fixed γ see Table 2). We will continue to discuss the anisotropy of the polymer chain on different length scales in the next section, when we analyze the static structure factor. Again we can plot the orientational resistance parameter m_G on a single master plot (see Figure 7), yielding $m_G \propto \beta_{\chi G}{}^{0.54\pm0.03}$. These results can be compared with experimental data obtained by light scattering of dilute polymer solutions,[5] but it should be noticed that the experimental data has been obtained under various polymer−solvent conditions, whereas during the simulations only the length of the chain has been varied. Similar to the case for m_A, we need the extrapolation scheme (see section 3) to determine m_G in the weak-flow-limit, from which we estimate $m_{G0} \approx 1.7$. The theoretical predictions for the constant coefficient m_G are summarized as follows: $m_G = 1.75$ (without HI[48]), $m_G = 2.5$ (preaveraged HI[38]), and $m_G = 1.7$ (derived from renormalization group studies[45]).

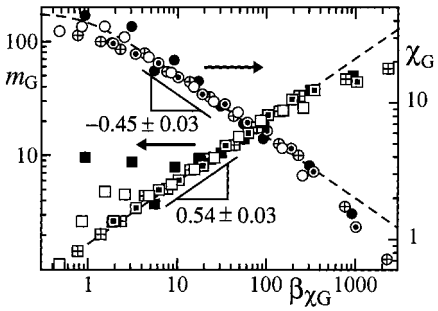

Figure 7. Master plot for the orientation angle χ_G (circles) and the orientation resistance m_G (boxes) versus the reduced shear rate $\beta_{\chi G} = \tau_{\chi G}\gamma$ for various chain lengths (style of symbols as in Figure 2). For shear rates $\beta_{\chi G} \geq 2$ both quantities follow a power law, i.e. $\chi_G \propto \beta_{\chi G}{}^{-0.45\pm0.03}$ and $m_G \propto \beta_{\chi G}{}^{0.54\pm0.03}$.

A value of $m_{G0} \approx 2.1$ has been reported from light-scattering experiments in the linear flow regime,[5] whereas a previous NEMD study[16] suggests $m_{G0} \approx 2$. (This value has not been reported by the authors.)

Chain Deformation. It was observed experimentally that the shear rate dependence of the orientational resistance parameter varies with the polymer−solvent, but the increase occurs independent of the solvent quality;[5] i.e., the contribution of hydrodynamic interactions and excluded volume to this effect are small. Obviously, the main contribution stems from the finite extendability of both the polymer coil and its subparts, which is in accordance with recent analytical calculations.[43] It becomes evident when analyzing the shear-induced increase (or decrease) of the diagonal elements of the tensor of gyration. The deformation of the chain can be measured via the diagonal elements G_Λ ($\Lambda = xx$, yy, zz) of the tensor of gyration via $\Delta G_\Lambda = |G_\Lambda/G_{\Lambda 0} - 1|$ with the equilibrium value $G_{\Lambda 0} = r_G{}^2/3$. The results of the scaling procedure are summarized in Table 5.

The results obtained for the deformation rates ΔG_Λ quantify the observed stretching of the chain in the flow direction, its compression into the gradient direction and, less pronounced, in the vorticity direction.

Table 5. Characterization of the Master Curves for the Deformation Rates ΔX with $X = r_G^2$, $X = G_\Lambda$, and $X = A_\Lambda$ ($\Lambda = xx, yy, zz$)[a]

	$\tau_X = bN^\alpha$		$\Delta X = d\beta_X^\mu$ ($\beta_X < 1$)	
ΔX	b	α	d	μ
Δr_G^2	0.015 ± 0.010	2.8 ± 0.3	0.20 ± 0.05	1.4 ± 0.2
ΔG_{xx}	0.06 ± 0.01	2.6 ± 0.2	0.6 ± 0.2	1.9 ± 0.2
ΔG_{yy}	0.25 ± 0.10	1.5 ± 0.1	0.5 ± 0.1	1.2 ± 0.2
ΔG_{zz}	0.03 ± 0.02	1.8 ± 0.3	0.5 ± 0.2	0.7 ± 0.2
ΔA_{xx}	0.25 ± 0.01	1.3 ± 0.1	1.4 ± 0.2	1.8 ± 0.2
ΔA_{yy}	0.29 ± 0.02	1.2 ± 0.1	1.0 ± 0.2	1.5 ± 0.2
ΔA_{zz}	0.14 ± 0.05	1.3 ± 0.2	0.7 ± 0.3	1.4 ± 0.3

[a] The table specifies the power laws. Note that $\Delta X = d\beta_X^\mu$ under the restriction $\beta_X < 1$.

In the weak flow regime we used power laws $\Delta G_\Lambda = d_\Lambda \beta_{G\Lambda}^\mu$ in order to fit the shear rate dependence of the Λ-diagonal element of **G** ($\mu = 1.9 \pm 0.2$, 1.2 ± 0.2, 0.7 ± 0.2 for $\Lambda = xx, yy, zz$, respectively). In *flow direction* the exponent is in good agreement with SANS data,[6] theoretical predictions,[38,50] and NEMD computer simulations.[16] Whereas in the *direction of flow gradient*, theoretical approaches predict either no[38] or a rather small deformation rate, e.g., $\Delta G_{yy} = -0.0069\beta^2$.[50] From an earlier simulation study $\Delta G_{yy} \approx -0.15\beta^2$ has been reported.[16] A compression in the *vorticity direction* has been detected experimentally[6] too but not yet taken into account in an analytic theoretical description, as far as we know. In contrast to theoretical approaches on Hookean bead−spring models,[38,50] our description of ΔG_Λ in terms of power laws is limited to rather small shear rates, since in the strong flow regime further stretching or compression of the chain is drastically reduced. The occurrence of saturation effects is in agreement with SANS experiments[6] as well as NEMD studies with fixed bond lengths[16] and indicates that the main contribution of this effect stems from the finite segment length. This interpretation is confirmed by recent theoretical approaches which take finite extendability explicitly into account.[43,51] It also explains that the scaling procedure used here does not lead to N-independent master plots, which approximate the deformation rates in both the weak and the strong flow regime. Therefore we restricted ourselves to scaling the data for ΔG_Λ at rather small shear rates, where ΔG_Λ seems to be unaffected by the type of binding potential. As for other properties we can express the relaxation time by $\tau_{G\Lambda} = bN^\alpha$. The prefactor b is fixed by the range of validity of the weak flow behavior; i.e. the deformation rate obeys $\Delta G_\Lambda \propto \beta_{G\Lambda}^\mu$ up to $\beta_{G\Lambda} = 1$. According to this scheme we cannot interpret $\tau_{G\Lambda}$ as a relaxation time as for other properties, since the value of b (but not the exponent α) depends on the finite extendability of segments and the chain length. We find the exponent α to show a significant dependence of the direction of deformation, i.e., $\alpha = 2.6 \pm 0.2$, 1.5 ± 0.1, and 1.8 ± 0.3 in direction x, y, z (see Table 5).

In order to compare our results with the light-scattering data presented by Link,[29] we averaged and analyzed the shape of the polymer relative to its principal axes (see Figure 8). For the amount of stretching in direction A (which has a large component in flow direction), we find $\Delta G_A \propto \beta_{GA}^\mu$ with $\mu \approx 1.9$ (expt range: $\mu = 1.8 \pm 0.2$). For direction B we find $\Delta G_B \propto \beta_{GB}^\mu \propto 1.1$ (expt range: $\mu = 1.0 \pm 0.2$). Since analytical models underestimate if not neglect the shear-induced compression of the polymer coil perpendicular to the flow direction, we find the deformation rate Δr_G to differ significantly from the theoretical predicted relationship $\Delta r_G \propto \beta^2$. From the simulation data we get $\Delta r_G \propto \beta_{rG}^\mu$ with $\mu = 1.4 \pm 0.3$ (expt range: $\mu = 1.3 \pm 0.1$).

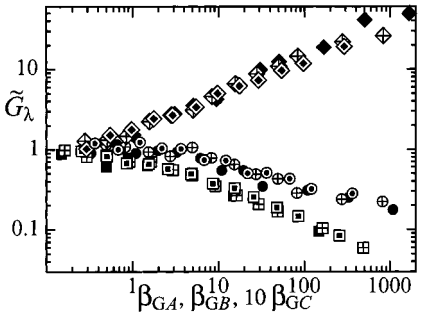

Figure 8. Normalized eigenvalues of the gyration tensor $\tilde{G}_\lambda = G_\lambda / r_{G0}^2$ versus $\beta_{G\lambda}$ (see Table 4) for various chain lengths (style of symbols as in Figure 2) and the three principal axes, $\lambda = A$ (diamonds), B (boxes), and C (circles). The eigenvalue $\tilde{G}_C$, which measures the deformation of the polymer chain perpendicular to the shearing plane, is unaffected by flow only at (low) shear rates $\beta_{GC} \leq 5$.

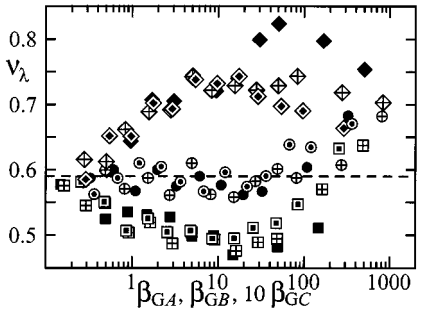

Figure 9. The exponents ν_λ describing the slope of $\tilde{S}(k_\lambda) = S(k_\lambda)/S(0)$ versus $\beta_{G\lambda}$ for $\lambda = A$ (diamonds), B (boxes), and C (circles). The style of symbols mark different chain lengths with the same notation as in Figure 2.

Anisotropy of the Static Structure Factor. Under flow conditions, the static structure factor becomes also anisotropic. In order to discuss its shape we will present values for the structure factor as measured along the principal axes of **G** (see eq 15). As in equilibrium for any principal axis $\lambda = A, B, C$, an exponent ν_λ, can be extracted from $S(k_\lambda) \propto k_\lambda^{-1/\nu_\lambda}$ with k_λ restricted to an interval which is specified below. Values for ν_λ are summarized in Figure 9 and Table 3. When plotting the curves, the relaxation times $\tau_{G\lambda}$ were used (see Table 4 for details). Previously we reported $\nu_{A,B,C} = \nu_{eq} \approx 0.58$ in equilibrium. With increasing shear rate, ν_A increases and reaches the limiting values $\nu_A = 0.72$ (for $N = 10$ and $\gamma = 0.2$) and $\nu_A = 0.82$ (for $N = 60$ and $\gamma = 0.03$). In contrast, ν_B decreases and reaches the lower limiting values $\nu_B = 0.52$ ($N = 10$, $\gamma = 0.3$) and $\nu_B = 0.47$ ($N = 60$, $\gamma = 0.03$). Perpendicular to the shear plane only a slight decrease is found, $\nu_C = 0.56-0.58$ for $\gamma \leq 0.1$. Above the limiting rates mentioned, the tendencies are reversed and the exponents may even cross their equilibrium value. Such behavior has been also reported for bead−rod chains by Pierleoni and Ryckaert.[16] They showed that the anisotropic structure factors, i.e., its values along the principal axes $\lambda = A, B, C$, obey (approximately) the scaling relation

$$S(k_\lambda) \rightarrow S(\sqrt{G_\lambda} k_\lambda)/N = F_S(k_\lambda) \qquad (21)$$

at fixed β, whose degree of validity—for our simulation

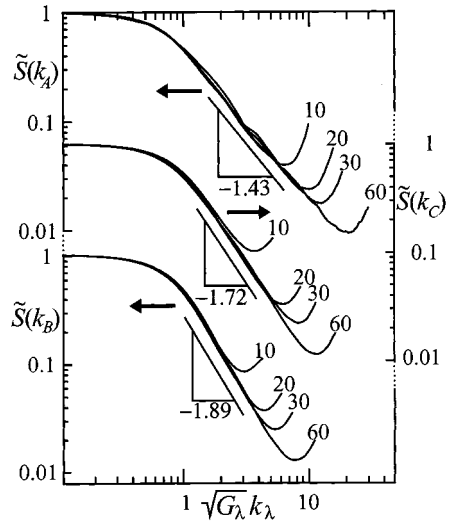

Figure 10. NEMD data for the reduced rate $\beta_{G\lambda} = 5$. Scaling behavior of the normalized static structure factor $S(k_\lambda)$ versus $\sqrt{G_\lambda}k_\lambda$ for various chain lengths N and for the principal axes $\lambda = A$ (upper curves), B (centered curves), and C (lower curves). The power law $S(k_\lambda) \propto k_\lambda^{-1/\nu_\lambda}$ holds for all principal axes in the high-k_λ region, but various exponents ($\nu_A = 0.70 \pm 0.02$, $\nu_B = 0.53 \pm 0.02$ and $\nu_C = 0.58 \pm 0.03$) are involved.

data at $\beta_{G\lambda} = 5$—is demonstrated in Figure 10. The shear-induced anisotropy of the intramolecular pair correlation function leads to the observed shear rate dependence of the scaling exponents ν_λ. The corresponding correlation length increases with shear rate in flow direction A ($\nu_A > \nu_{eq}$), but decreases in direction B ($\nu_B < \nu_{eq}$) while it is quite unaffected in the vorticity direction ($\nu_C \approx \nu_{eq}$) for low rates. The exponent ν_λ is estimated from the reduced wave number interval $k_{\lambda 1} \equiv 1.5\sqrt{G_\lambda} < k < 2.2/\sqrt{a_\lambda} \equiv k_{\lambda 2}$. The presence of a weak flow mainly affects the values for G_A and G_B, which cause k_{A1} to decrease and k_{B1} to increase, while k_{C1}, $k_{\lambda 2}$, $S(k_{\lambda 1})$, and $S(k_{\lambda 2})$ remain unchanged. In accordance with the increase of local anisotropy at high shear rates, $k_{\lambda 2}$ varies with shear rate, and consequently, with increasing local anisotropy, k_{A2} (k_{B2}) is shifted to smaller (higher) values. In addition, the local correlations increase along direction A since $S(k_{A2})$ decreases. On the other hand, the correlations decrease in the direction of B since here, the extension of the polymer chain is drastically reduced; i.e., $S(k_{B2})$ increases. Both mechanisms together lead to the reported flow-induced changes of ν_λ. In general, in order to interpret the exponents ν_A and ν_B, one has to notice that the static structure factor exhibits k-dependent rotation of its elliptic isoclines. Similar behavior has been observed in sheared polymer melts via NEMD and SANS.[18,52] For the related angle we detect values which lie in between these for the flow alignment angles χ_G (at small k values, the Guinier regime) and χ_A (large k values).

D. Rotational Dynamics of the Polymer Chain. For fluids subjected to a simple shear flow (plane Couette geometry) one has $\nabla \times \mathbf{v} \neq 0$, and hence the torque balance leads to a nonvanishing angular velocity ω perpendicular to the plane of flow. As shown earlier for rigid rodlike and ellipsoidal particles[53,54] under shear flow, the measured steady alignment of suspended particles results from their unsteady, flow-induced rotation. Obviously, in order to describe the rotation of chains subjected to shear flow, the conformational freedom of the flexible polymer chain has to be "added"

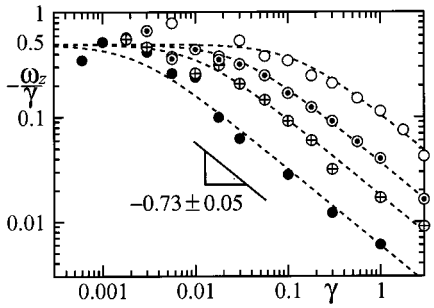

Figure 11. The reduced angular velocity $-\omega_z/\dot{\gamma}$ versus $\dot{\gamma}$ for various chain lengths (symbols as in Figure 2) decreases with shear rate, starting from the value 0.5, which has been predicted by analytic theories for rigid and ideal elastic chains (see section 4).

to this description.[55,56] For its time-averaged value one expects $\omega = (0, 0, -0.5\dot{\gamma})$ for rigid rods as well as for ideal flexible chains.[57,58] Qualitatively different behavior was predicted by "internal viscosity" models (IVM)[59,60] for polymer chains in dilute solutions. On the basis of an appropriate orientational diffusion equation the authors determined the strength of decrease of angular velocity with shear rate.

The angular velocity ω as evaluated during the simulation is given by

$$\omega \equiv \Theta^{-1} \cdot \mathbf{d} \tag{22}$$

Here, $\Theta \equiv (N r_G^2\, \mathbf{1} - \mathbf{G})$ denotes the tensor of inertia of the polymer chain and

$$\mathbf{d} \equiv \frac{1}{N}\sum_{i=1}^{N}(\mathbf{r}_i - \mathbf{r}_{cm}) \times \mathbf{c}_i \tag{23}$$

its angular momentum, where $\mathbf{c}_i \equiv \mathbf{v}_i - \mathbf{v}(\mathbf{r}_i)$ is the peculiar velocity of particle i and $\mathbf{r}_{cm}$ stands for the center of mass coordinates of the polymer chain. The investigation of the angular velocity by our NEMD simulations turned out to be a difficult task, since the peculiar velocity in eq 22 is dominated by the thermal contribution, which is on the same order of magnitude at any shear rate. In order to obtain reasonable statistics for any set, the peculiar velocities were averaged over a finite time interval (20−60 integration time steps), which is on the order of the thermal relaxation time of segments (local) but small compared to the rotational relaxation time of the polymer coil. As depicted in Figure 11, the predicted behavior of the angular velocity is found at low shear rates. Above $\beta_\omega = 1$ this relationship is violated and $-\omega_z/\dot{\gamma}$ decreases with increasing rate, in agreement with IVM models calculated for an internal viscosity parameter of order unity.[60] For the rotational dynamic process our extraction scheme provides the relaxation times $\tau_\omega = (0.05 \pm 0.01)N^{2.2\pm0.2}$ as obtained from $\tau_\omega[N] = 8 \pm 1$, 35 ± 4, 95 ± 10, and 400 ± 40 for $N = 10$, 20, 30, 60, respectively.

5. Summary and Conclusions

In this work a FENE polymer chain in solution is studied via nonequilibrium molecular dynamics. The influence of shear flow on rheological and conformational properties is analyzed for various chain lengths in great detail, allowing one to specify accurate analytical expressions for the flow curves of most quantities. Within the simulation all the rheological quantities were

simultaneously accessible and their behavior resembles qualitatively that found for real polymer solutions. Emphasis was laid on the underlying microstructural changes, i.e., shear-induced alignment of the segments, the characteristic elliptical distortion of the polymer coil, and the scaling exponents characterizing the rheo-optical features of the model polymer solution. Whenever possible the results were compared with experimental and theoretical findings. The main conclusions from this investigation are summarized as follows:

(i) Equilibrium Limit. In the limit of weak flow the conformational properties of the chain are the same as obtained by previous MD simulations[14] and their dependence of chain length is in accordance with the theoretical predicted power laws. The hydrodynamic behavior, i.e., the finite box-size corrected data of the chain diffusion constant D and the hydrodynamic radius, is consistent with the Kirkwood−Riseman theory. Hence, the monomer diffusion constant is independent of the chain length. For the diffusion constant D and the corresponding relaxation time τ_D we found good quantitative agreement with predictions of the Zimm model.

(ii) Rheological Behavior. An effect of chain length on the shear viscosity was detected for the intrinsic viscosity, which was extracted from the intramolecular interactions, but unfortunately not for the solution viscosity, due to the poor quality of the statistical resolution. We observe a shear modulus which is dependent on chain length, i.e., the scaling $\eta^2/\Psi_1 \propto N^0$, as predicted, for example in ref 45, does not apply (see Table 4). The normal stresses produced by the pure solvent are negligible small compared to those measured for the model polymer solution. Thus, they serve as a sensitive measure of the influence of the polymer chain on the solution viscometric functions and give a more precise estimate than that determined by measuring the shear viscosity of the polymer solution. A study of intrinsic viscosities obtained by modified microscopic definitions, such as an intrinsic stress tensor which takes polymer−solvent interactions into account, is in progress. Its importance for the interpretation of simulation data for our model lies in the fact that the solvent itself behaves non-Newtonianly above shear rates $\gamma \approx 0.3$ with respect to shear viscosity.

(iii) Stress-Optical Rule. The proportionality between intrinsic stress and alignment tensor was verified at small and intermediate shear rates. However, violations were observed in the strong flow regime, but only at shear rates much higher than those used in birefringence experiments. These deviations were related to the flow-induced changes of the distribution of bond lengths, which is particularly affected by the FENE potential.

(iv) Orientational Anisotropy. The flow-alignment angles χ_A and χ_G, which are experimentally accessible via flow birefringence and light-scattering measurements,[2,4,5,44,45] have been shown to scale with chain size N and shear rate (see Table 4), in agreement with experimental findings. It has been demonstrated that, in contrast to the commonly referenced theoretical predictions $\cot(2\chi) \propto \gamma$, the decrease of alignment angle $\chi(\gamma)$ with increasing shear rate is more pronounced at low rates and weaker at high rates. It should be noticed that this behavior can be interpreted by more recent theoretical approaches,[43,51] which also imply a shear rate dependence of the orientational resistance parameters m_G and m_A. As shown here, the orientational resistance parameters increase with shear rate. Its scaling behavior is reported in Table 4.

(v) Distortion of the Polymer Coil. The simulation data reveal characteristic elliptical distortions of the scattering pattern (from the individual chain) as observed from SANS experiments. The decay the static structure factor along the main axes $\lambda = A, B, C$ exhibit a significant dependence on the anisotropy of both the tensor of gyration and the alignment tensor. Its anisotropy is expressed here in terms of the exponent ν_λ as a function of shear rate and chain length. The measured k-dependence of the angle between the long axis of the ellipses and the gradient direction confirms the picture in which the molecular anisotropy at a local scale of the chain is lower than the anisotropy of the end-to-end tensor or tensor of gyration. The deformation rates of the tensor of gyration calculated from its diagonal elements increase in flow direction (x) and decrease in the direction of velocity gradient (y) and the one perpendicular to the shear plane (z). In the weak flow regime along the x axis, our data is in qualitative agreement with theory and experiment. In both y and z direction we find the deformation (compression) of the polymer chain to be more pronounced, in contrast to most theoretical predictions but in agreement with experimental findings and recent NEMD simulations on bead−rod chains. At high shear rates the deformation ratios approach a saturation regime due to the rather small length of the chain and the limited extendability of its segments, which is also confirmed by scattering experiments.

(vi) Rotational Dynamics. In accordance with predictions of IVM models, the ratio of the time-averaged angular velocity of the polymer chain ω_z and shear rate decreases in the strong flow regime. In these models, this behavior stems from a deformation force which changes its value under flow in order to conserve a symmetric stress tensor.[59,60] In the simulation we observe a correlation between strong (weak) alignment and large (small) deformation of the chain. For example, during the time the main axis of the tensor of gyration lies parallel to the flow gradient direction, its mean shape tends to become spherical, and the coupling of the chain to the macroscopic flow field is decreased in comparison with the opposite state, where the main axis is parallel to the flow direction. These mechanisms produce an unsteady angular velocity and reduce the ratio, ω_z/γ, whose dependence on shear rate and chain length has been quantified here.

(vii) Molecular Dynamics versus Brownian Dynamics. The results of the presented molecular dynamics study may be used to check or refine Brownian molecular dynamics algorithms, which do not consider hydrodynamic interactions via explicit solvent particles. This is especially true for high shear rates, where the Brownian dynamics method tends to fail.[19] Hence, the results will serve to determine an upper limit for a reasonable maximum shear rate for Brownian dynamics studies of the FENE chain model.

(viii) Relaxation Times. The evaluation scheme introduced in section 3 enables us to determine relaxation times τ_X independently for almost all measured quantities X. Even for the rather short chains ($10 \leq N \leq 60$) investigated here, the chain length dependence of τ_X for fixed X is found to obey power laws, e.g., $\tau_\eta \propto N^{1.6}$ for $X = \eta^{int}$ (see Table 4 for details). In contrast to theoretical predictions, these power laws depend on the

chosen quantity X, reflecting the underlying influence of relaxation processes which act on different length scales. Although the exponents and prefactors vary from quantity to quantity, there exist obvious interrelations, e.g., $\tau_\eta \approx \tau_{A\eta} \approx \tau_{G\eta}$ and $\tau_{\chi G} \approx 2\tau_{\chi A}$.

According to the good agreement of simulation and experimental results, the bead−FENE−spring chain model used here is a reasonable alternative to bead−rod and bead−harmonic spring models for further investigations, e.g. if other flow geometries and concentrations are considered. In contrast to previous approaches the simulation provides also information about property-specific relaxation times determined from flow curves, which can be compared with the corresponding correlation times calculated from time series.

Acknowledgment. The author C.A. thanks the Graduiertenkolleg "Polymerwerkstoffe" (Berlin) of the Deutsche Forschungsgemeinschaft for financial support. We thank the Konrad-Zuse-Zentrum für Informationstechnik (Berlin) for their generous donation of CPU time on their CRAY Y-MP 4D/464. The author M.K. acknowledges financial support by the Minerva-foundation, Munich.

References and Notes

(1) Bird, R. B.; Hassager, O.; Armstrong, R. C.; Curtiss, C. F. *Dynamics of Polymeric Liquids*; John Wiley & Sons: New York, 1987; Vols. 1 and 2.
(2) Janeschitz-Kriegl, H. J. *Adv. Polym. Sci.* **1969**, *6*, 170.
(3) Peterlin, A. *Annu. Rev. Fluid Mech.* **1976**, *8*, 35.
(4) Cottrell, F. R.; Merrill, E. W.; Smith, K. A. *J. Polym. Sci. A-2* **1969**, *7*, 1415.
(5) (a) Link, A.; Zisenis, M.; Prötzl, B.; Springer, J. *Makromol. Chem., Macromol. Symp.* **1992**, *61*, 358. (b) Zisenis, M.; Springer, J. *Polymer* **1995**, *36*, 3459.
(6) (a) Lindner, P.; Oberthür, R. C. *Coll. Polym. Sci.* **1988**, *266*, 886. (b) Lindner, P.; Oberthür, R. C. *Physica B* **1989**, *156&157*, 410.
(7) Doi, M.; Edwards, S. F. *The Theory of Polymer Dynamics*; Clarendon Press: Oxford, 1986.
(8) de Gennes, P.-G. *Scaling Concepts in Polymer Physics*; Cornell University Press: Ithaca, NY, 1979.
(9) de Gennes, P.-G. *Macromolecules* **1976**, *9*, 587, 594.
(10) des Cloizeaux, J.; Jannink, G. *Polymers in Solution: Their Modelling and Structure*; Clarondon: Oxford, 1990.
(11) Hoover, W. G. *Physica A* **1993**, *194*, 450.
(12) Kremer, K.; Grest, G. S. *J. Chem. Phys.* **1990**, *92*, 5057.
(13) Dünweg, B.; Kremer, K. *Phys. Rev. Lett.* **1991**, *61*, 2996.
(14) Dünweg, B.; Kremer, K. *J. Chem. Phys.* **1993**, *99*, 6983.
(15) (a) Pierleoni, C.; Ryckaert, J.-P. *Phys. Rev. Lett.* **1991**, *61*, 2992. (b) Pierleoni, C.; Ryckaert, J.-P. *J. Chem. Phys.* **1992**, *96*, 8539.
(16) Pierleoni, C.; Ryckaert, J.-P. *Macromolecules* **1995**, *28*, 5097.
(17) Hess, S. *J. Non-Newtonian Fluid Mech.* **1987**, *23*, 305.
(18) Kröger, M.; Loose, W.; Hess, S. *J. Rheol.* **1993**, *37*, 1057.
(19) Öttinger, H. C. *Stochastic processes in polymeric fluids*; Springer, Berlin, 1996.
(20) López Cascales, J. J.; Navarro, S.; Garcia de la Torre, J. *Macromolecules* **1992**, *25*, 3574.
(21) Knudsen, K. D.; Elgsaeter, A.; López Cascales, J. J.; Garcia de la Torre, J. *Macromolecules* **1993**, *26*, 3851.
(22) (a) Carl, W. Modellrechnungen an Polymerlösungen im Schergefälle Ph.D. Thesis, D83, Technische Universität Berlin, 1992. (b) Carl, W. *Macromolecules* **1993**, *26*, 557.
(23) Weeks, J. D.; Chandler, D.; Andersen, H. C. *J. Chem. Phys.* **1971**, *54*, 5237.
(24) Hess, S.; Kröger, M.; Voigt, H. *Physica A* **1998**, *250*, 58.
(25) Warner, H. R. *Ind. Eng. Chem. Fundam.* **1972**, *11*, 379.
(26) These values have been determined from the transition in zero-shear-rate of the power laws in NEMD simulations of polymer melts. See: Kröger, M. *Rheology 95* **1995**, *5*, 66.
(27) Lees, A. W.; Edwards, S. F. *J. Phys. C* **1972**, *5*, 1921.
(28) Hoover, W. G. *Molecular Dynamics*; Lecture Notes in Physics 258; Springer: New York, 1986.
(29) Link, A. Konformation und Ausrichtung von Makromolekülen in der Scherströmung. Ph.D. Thesis, D83, Technische Universität Berlin, 1992.
(30) Peterlin, A.; Heller, W.; Nakagaki, M. *J. Chem. Phys.* **1958**, *28*, 470.
(31) (a) Ostwald, W. *Kolloid-Z.* **1925**, *36*, 99. (b) de Waele, A. *Oil Color Chem. Assoc. J.* **1923**, *6*, 33.
(32) Yasuda, K.; Armstrong, R. C.; Cohen, R. E. *Rheol. Acta* **1981**, *20*, 163.
(33) Kirkwood, J. G.; Riseman, J. *J Chem. Phys.* **1948**, *16*, 565.
(34) Hansen, J. P.; McDonald, I. R. *Theory of simple liquids*; Academic Press: London, 1986.
(35) Staudinger, H. *Ber. Dtsch. Chem. Ges.* **1930**, *63*, 222.
(36) Huggins, M. L. *J. Chem. Phys.* **1938**, *42*, 911.
(37) Elias, H.-G. *An Introduction to Polymer Science*; Wiley-VCH: Weinheim, 1997.
(38) Zimm, B. H. *J. Chem. Phys.* **1956**, *24*, 269.
(39) Flory P. J. *Statistical mechanics of chain molecules*; Wiley-Interscience: NY, 1969.
(40) Kuhn, W. *Kolloid Z.* **1934**, *68*, 2.
(41) Bird, R. B.; Dotson, P. J.; Johnson, N. L. *J. Non-Newton. Fluid Mech.* **1980**, *7*, 213.
(42) Carl, W. *Macrom. Theory Simul.* **1994**, *3*, 705.
(43) Winkler, R. G. Analytical description of finite size effects for chain molecules in shear flow. Submitted, 1997.
(44) Janeschitz-Kriegl, H. J. *Polymer melt rheology and flow birefringence*; Springer: Berlin, 1983.
(45) (a) Bossart, J.; Öttinger, H. C. *Macromolecules* **1995**, *28*, 5852. (b) Bossart, J.; Öttinger, H. C. *Macromolecules* **1997**, *30*, 5527.
(46) (a) Kuhn, W. *Kolloid Z.* **1936**, *76*, 258. (b) Kuhn, W. *Kolloid Z.* **1939**, *87*, 3. (c) Kuhn, W.; Grün, F. *Kolloid Z.* **1942**, *101*, 248.
(47) de Gennes, P.-G. *The Physics of Liquid Crystals*; Clarendon Press: Oxford, 1974.
(48) Rouse, P. E. *J. Chem. Phys.* **1953**, *21*, 1272.
(49) (a) Öttinger, H. C. *J. Chem. Phys.* **1987**, *86*, 3731. (b) Öttinger, H. C. *Phys. Rev. A* **1989**, *40*, 2664.
(50) Wang, S. Q. J. *J. Chem. Phys.* **1990**, *92*, 7618.
(51) Schneggenburger, C.; Kröger, M.; Hess, S. *J. Non-Newtonian Fluid Mech.* **1996**, *62*, 235.
(52) Muller, R.; Pesce, J. J.; Picot, C. *Macromolecules* **1993**, *26*, 4356.
(53) Jeffrey, G. B. *Proc. R. Soc. London, Ser. A* **1922**, *102*, 161.
(54) Peterlin, A.; Stuart, H. A. *Hand- Jahrbuch d. Chem. Phys.* **1943** *8*, 113.
(55) Kuhn, W. *Z. Phys. Chem. A* **1932**, *161*, 1.
(56) (a) Peterlin, A. *Z. Phys.* **1938**, *111*, 232. (b) Peterlin, A.; Stuart, H. A. *Z. Phys.* **1939**, *112*, 1.
(57) Debye, P. *J. Chem. Phys.* **1946**, *14*, 636.
(58) Peterlin, A. *J. Polym. Sci. A-2* **1967**, *5*, 179.
(59) Cerf, R. *J. Chim. Phys.* **1969**, *66*, 479.
(60) (a) Bazúa, E. R.; Williams, M. C. *J. Chem. Phys.* **1973**, *59*, 2858. (b) Bazúa, E. R.; Williams, M. C. *J. Polym. Sci., Polym. Phys. Ed.* **1974**, *12*, 825.

MA981683U